Magnetoelectric effect in antiferromagnetic multiferroic $Pb(Fe_{1/2}Nb_{1/2})O_3$ and its solid solutions with $PbTiO_3$

V. V. Laguta,[1,2] V. A. Stephanovich,[2] I. P. Raevski,[3] S. I. Raevskaya,[3] V. V. Titov,[3] V. G. Smotrakov,[3] and V. V. Eremkin[3]

[1]*Institute of Physics AS CR, Cukrovarnicka 10, 162 53 Prague, Czech Republic*

[2]*Institute of Physics, Opole University, Oleska 48, 45-052 Opole, Poland*

[3]*Research Institute of Physics and Faculty of Physics, Southern Federal University, Stachki Avenue 194, 344090 Rostov-on-Don, Russia*

(Received 30 November 2016; revised manuscript received 9 January 2017; published 25 January 2017)

Antiferromagnets (AFMs) are presently considered as promising materials for applications in spintronics and random access memories due to the robustness of information stored in the AFM state against perturbing magnetic fields. In this respect, AFM multiferroics may be attractive alternatives for conventional AFMs as the coupling of magnetism with ferroelectricity (magnetoelectric effect) offers an elegant possibility of electric-field control and switching of AFM domains. Here we report the results of comprehensive experimental and theoretical investigations of the quadratic magnetoelectric (ME) effect in single crystals and highly resistive ceramics of $Pb(Fe_{1/2}Nb_{1/2})O_3$ (PFN) and $(1-x)Pb(Fe_{1/2}Nb_{1/2})O_3-xPbTiO_3$(PFN-$x$PT). We are interested primarily in the temperature range of the multiferroic phase, $T < 150$ K, where the ME coupling coefficient is extremely large (as compared to the well-known multiferroic $BiFeO_3$) and shows sign reversal at the paramagnetic-to-antiferromagnetic phase transition. Moreover, we observe strong ME response nonlinearity in the AFM phase in the magnetic fields of only a few kOe. To describe the temperature and magnetic field dependencies of the above unusual features of the ME effect in PFN and PFN-xPT, we use a simple phenomenological Landau approach which explains experimental data surprisingly well. Our ME measurements demonstrate that the electric field of only 20–25 kV/cm is able to switch the AFM domains and align them with ferroelectric ones even in PFN ceramic samples.

DOI: 10.1103/PhysRevB.95.014207

I. INTRODUCTION

$Pb(Fe_{1/2}Nb_{1/2})O_3$ (PFN) and its solid solutions with $PbTiO_3$ (PT) and $PbZr_{1-x}Ti_xO_3$ (PZT) are among the most intensively studied multiferroic materials; see recent publications [1–5]. The disorder in PFN perovskite structure is due to the presence of two different ions, magnetic Fe^{3+} and nonmagnetic Nb^{5+}, at the same octahedral position. Nevertheless, it undergoes a quite normal ferroelectric phase transition at the temperature $T_C \approx 370$ K with large enough remanent polarization (see, e.g., Refs. [6,7]). On cooling, PFN undergoes antiferromagnetic (AFM) phase transition at the Néel temperature $T_N \approx 150$ K, and finally at low temperatures (11–12 K) it freezes into a spin-glass state which, however, coexists with the above-mentioned long-range ordered AFM phase. The latter coexistence has recently been studied in detail both experimentally and theoretically [3,8].

It is worth also noting that there are a number of publications in which room-temperature hysteresis loops with a weak magnetization have been reported for ceramics, nanopowders, and thin films of PFN [9–11] and its analog $Pb(Fe_{1/2}Ta_{1/2})O_3$ (PFT) [12,13]. As the Néel temperature of both PFN and PFT is well below room temperature [1–4,14], a possible origin of these room-temperature ferromagneticlike properties was supposed to be the formation of superparamagnetic clusters [10], Fe spin clustering [5], and the possible presence of a small admixture of parasitic ferromagnetic or ferrimagnetic phase such as $PbFe_{12}O_{19}$ [15]. As a rule, the amount of latter superparamagnetic or ferromagnetic phases is below the detection limit for x-ray diffraction and Mössbauer spectroscopy. At the same time, these phases can be well detected by magnetic resonance spectroscopy [2,16].

The magnetoelectric (ME) effect had been observed in PFN many years ago, starting from 1980. This was done mainly for single crystals and in the AFM phase [1,14,17]. We have found recently [18] that a sizable ME effect exists also in the paramagnetic (PM) phase of both PFN single crystals and ceramics as well as in PFN-PT solid solution ceramics. This ME effect disappears only in the paraelectric phase, where there is no spontaneous polarization. It is worth noting that while the linear ME effect in PFN is well researched [1,14], the quadratic ME coupling is much less studied despite its huge value ($\beta_{333} = 10^{-17} - 10^{-16}$ s/A [1,17]), which is almost three orders of magnitude larger than that in the well-known AFM multiferroic $BiFeO_3$($\beta_{333} = 2.1 \times 10^{-19}$ s/A [19,20]). The reason for this difference is still not clarified.

Large ME coupling in PFN, especially in ceramic samples, may be attractive for applications in ME memory elements and spintronics as AFM domains are almost unsusceptible to external magnetic fields which preserves well the stored information. The coupling between ferroelectricity and antiferromagnetism in PFN offers an intriguing possibility of electric field control and switching of AFM domains. Such electric-field switching of AFM domains has been demonstrated in $BiFeO_3$ single crystals [21].

Another important question which we want to clarify in this paper is the behavior of the ME coupling between disordered (dynamically or statically) spin ensemble and electric polarization in magnetoelectrics with spin-glass or superparamagnetic phases. In this context, the PFN diluted by PT is an almost ideal system as both ferroelectric and magnetic phases can be predictably modified by varying the Ti content in PFN-xPT solid solution [2,4,7].

Interestingly, the phenomenological Landau theory predicts the ME coupling increase on cooling proportional to the square of magnetic susceptibility [18,22]. Such an increase has not been experimentally observed in PFN [1], though its susceptibility increases substantially at temperatures below $T_N \approx 150$ K [2]. On the contrary, ME coupling was reported to decrease below the spin-glass freezing temperature $T_g \approx 11$ K [1].

In the present paper, we report the results of comprehensive investigations of the quadratic ME effect in crystals and highly resistive ceramics of $Pb(Fe_{1/2}Nb_{1/2})O_3$ and $(1-x)Pb(Fe_{1/2}Nb_{1/2})O_3$-$xPbTiO_3$. Usage of ceramic samples enables performing dielectric and ME response measurements up to the temperatures 400–450 K without marked influence of conductivity. We pay attention mainly to low ($T < 150$ K) temperatures, where the ME coupling coefficient is extremely large as compared, for instance, to $BiFeO_3$ and shows sign reversal at the paramagnetic-to-antiferromagnetic phase transition. Moreover, we observed strong ME response nonlinearity in the AFM phase in the fields of only a few kOe. We also present the results of ME measurements in PFN ceramics with 90° and 180° switching of electric polarization in the AFM phase which demonstrate that the alignment of electric domains leads to corresponding alignment of magnetic domains. To describe the temperature and magnetic field dependencies of the ME effect we use a simple Landau theory of phase transitions which explains experimental data surprisingly well.

The plan of our paper is the following. After a short description of the applied experimental methods (Sec. II), we report on our experimental exploration of the ME effect firstly in pure PFN (both single crystals and ceramics, Sec. III A) and then in PFN-PT solid solutions (Sec. III B). Section IV presents phenomenological theory of the quadratic ME coupling in both paramagnetic and AFM phases. Finally, in Secs. V and VI, we discuss the results obtained and make conclusions.

II. EXPERIMENT

Single crystals of PFN-xPT at $x = 0$, 0.03, and 0.2 were grown by spontaneous crystallization from the PbO-B_2O_3 flux in the temperature range from 1010 °C down to 850 °C (see Refs. [2,23] for details). The fabricated crystals were cubic shaped with the edges up to 4–6 mm and the faces parallel to (100) planes of the prototype perovskite structure. Chemical composition of the crystals obtained has been determined by the electron probe x-ray microanalyzer "Camebax-Micro," using PFN and $PbTiO_3$ as reference samples. In our measurements, crystals were cut either along (111) or (100) planes depending on the spontaneous polarization direction.

Ceramic samples of PFN-xPT ($x = 0$, 0.05) solid solution have been fabricated by the solid-state reaction route using high-purity Fe_2O_3, Nb_2O_5, PbO, and TiO_2. These oxides were batched in stoichiometric proportions and 1 wt % of Li_2CO_3 was added to the batch. This addition promotes formation of the PFN perovskite modification and inhibits conductivity [24]. The sintering has been performed at 1030 °C−1070 °C for 2 h in a closed alumina crucible. The density of the obtained ceramics was about 92%−97% of the theoretical one. X-ray diffraction analysis showed that all investigated compositions were single phase and had a perovskite-type structure.

Typical sample size for ME measurements was $2.5 \times 5 \times 0.9$ mm^3. The electrodes for measurements were deposited by silver paint (SPI Supplies, USA). Before the ME measurements, ceramic samples were poled at room temperature by dc electric field of 10 kV/cm for 10 min. Single crystals were poled at $T = 77-180$ K to avoid influence of conductivity which makes crystal poling at higher temperatures impossible. Poled samples were tested by measuring the piezoelectric coefficient, d_{31}, by the standard resonance-antiresonance method.

The ME coefficient was determined by a dynamic method [25] as a function of bias magnetic field H at a small ac field $h = 1-5$ Oe and frequencies 0.2–1 kHz (at these low frequencies ME response did not depend on frequency) by measuring the voltage across the sample utilizing a lock-in amplifier with a high-impedance preamplifier. Both ac and dc magnetic fields were applied normally to the surface of the sample with electrodes. In every ME experiment, more than two runs were repeated with the direction of H reversed and the change of the signal sign was confirmed. In this way, a possible spurious signal was segregated from a true ME one whose sign is dependent on the PH product.

In our experiment, the ME effect is manifested as a polarization P induced by a small ac magnetic field h_{ac} under application of dc field H_{dc} [25,26]. The magnetic field induced components of the polarization can be obtained from the free-energy expansion [27]:

$$F(\bar{E},\bar{H}) = F_0 - P_i^s E_i - M_i^s H_i - \frac{1}{2}\varepsilon_0\varepsilon_{ij}E_iE_j - \frac{1}{2}\mu_0\mu_{ij}H_iH_j - \alpha_{ij}E_iH_j - \frac{1}{2}\beta_{ijk}E_iH_jH_k - \cdots, \quad (1a)$$

$$P_i = -\frac{\partial F}{\partial E_i} = P_i^s + \varepsilon_0\varepsilon_{ij}E_j + \alpha_{ij}H_j + \frac{1}{2}\beta_{ijk}H_jH_k + \cdots, \quad (1b)$$

where $i,j,k = x,y,z$ are Cartesian coordinates, P^s and M^s are, respectively, the spontaneous polarization and magnetization; μ_{ij} and ε_{ij} are, respectively, magnetic and dielectric permittivities (μ_0 and ε_0 are the vacuum permittivities in SI units); α_{ij} and β_{ijk} are linear and linear-quadratic ME coupling coefficients, respectively. Using collinear dc and ac magnetic fields $H = H_{dc} + h\sin\omega t$, the first harmonic amplitude of the ac polarization detected by lock-in detector is

$$P_i(T) = \alpha_{ij}(T)h_j + \beta_{ijj}(T)H_jh_j. \quad (1c)$$

Since the linear ME coupling in PFN is much smaller than the quadratic one [14] and we are interested primarily in the quadratic ME effects, we neglect the α term hereafter. Technically, the quadratic ME effect is described by a third-rank tensor β_{ijk} for the arbitrary orientations of polarization and magnetic field vectors. In our experimental geometry, when both magnetic field and polarization are aligned along one crystallographic direction ([111] or [100] depending on

the spontaneous polarization direction), the measured ME coefficient is β_{333}. Obviously, only an effective coupling constant β_{333}, which represents an average of the different elements of the β_{ijk} tensor, should be considered in ceramics. For simplification, we will omit indices in the β_{333} element. Note that a microscopic theory of the quadratic ME effect for C_{3h} symmetry has been presented in Ref. [28].

The ME response was measured as the voltage induced by the ac polarization in a sample. The ME voltage is determined from Eq. (1b) as

$$U_{\mathrm{ME}} = \frac{dP_{\mathrm{ac}}}{dt}(\omega C + 1/R_i)^{-1} \approx \frac{\beta H_{\mathrm{dc}} h S}{C}, \qquad (2)$$

where C and S are the samples' capacitance and area, respectively. The expression for U_{ME} is valid under the condition $(\omega C)^{-1} \ll R_i$, where $R_i \sim 10^9 \Omega$ is the impedance of a lock-in amplifier with preamplifier. This relation is always fulfilled at the frequencies 0.2–1 kHz due to high capacitance of the samples.

III. EXPERIMENTAL RESULTS

As the dielectric and magnetic properties of our PFN single crystals and ceramics have been studied previously (see, e.g., Refs. [2,6,7]), here we present the results of ME effect measurements only. Also, here we primarily use the PFN-xPT solid solution crystals because ceramic samples contained ferromagnetic or superparamagnetic impurity phases, which masked intrinsic ME response at low magnetic fields.

A. ME effect in PFN crystals and ceramics

Figure 1(a) shows temperature dependence of the ME voltage measured in PFN crystal when a magnetic field is parallel to spontaneous polarization, aligned along the [111] crystal direction. One can see that the ME response strongly increases on cooling below the Néel temperature and changes sign at the transition from PM to AFM phase. Note that a similar effect has been observed previously (in measurements of electric-field-induced ME moment) but with lower resolution [1]. The sign change of the ME voltage is well seen in highly resistive PFN ceramics [Fig. 1(b)]. In ceramic samples, the ME signal can be measured up to the temperature of ferroelectric (FE) phase transition as it was demonstrated in Ref. [18]. Note that the quadratic ME coefficient in the AFM phase of PFN ($\beta_{333} = 2.5 \times 10^{-17}$ s/A in a crystal at $T = 10$ K and $\beta = 1.0 \times 10^{-16}$ s/A in ceramics at $T = 20$ K) is two to three orders of magnitude higher than that in $BiFeO_3$ crystal ($\beta_{333} = 2.1 \times 10^{-19}$ s/A at $T = 4.2$ K [19]). Such a large ME coefficient in PFN ceramics indicates that the sublattice magnetization is preferably aligned along electric polarization so that magnetization can in principle be switched by an electric field in AFM phase.

The data in Fig. 1 also suggest that the paramagnetoelectric (PME) contribution is nonzero in the magnetically ordered phase. It competes with the ME contribution related to AFM order parameter which has the opposite sign. This is well seen in ceramics, where the inversion point is shifted to about 100 K due to lower Néel temperature typical of Li-doped PFN ceramics [29]. These two contributions to the ME response in the free-energy expansion have the following form [18] (see also Sec. IV, below):

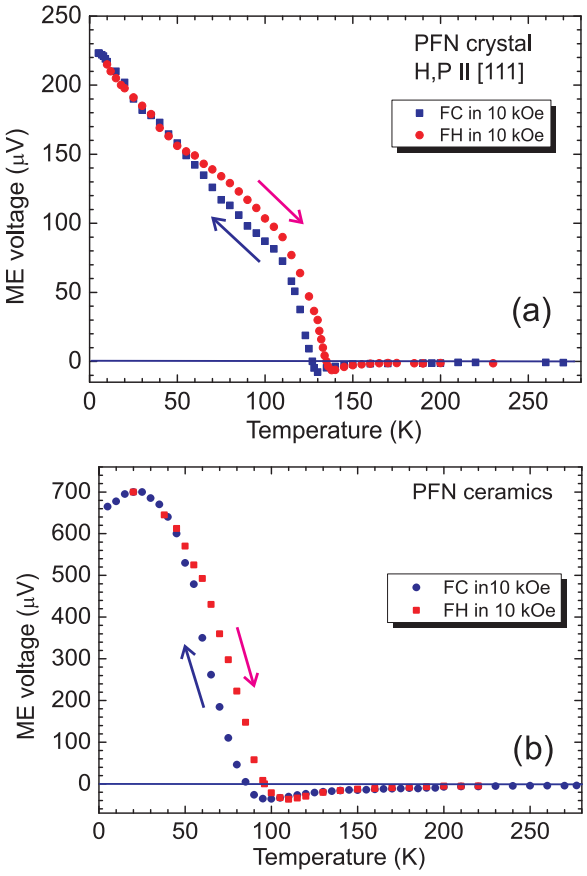

FIG. 1. Temperature dependence of the ME voltage measured in poled PFN crystal (a) and ceramics (b) in the field cooling (FC) and field heating (FH) modes under the field of 10 kOe. The magnetic field H is applied parallel to the electric polarization P.

$$G_{\mathrm{ME}} = \tfrac{1}{2}(\xi_{MP} M^2 + \xi_{LP} L^2) P^2. \qquad (3)$$

Here L is the AFM order parameter and ξ_{MP} and ξ_{LP} are biquadratic ME coefficients that couple corresponding order parameters.

Essentially nonlinear dependence of ME response on applied field in the AFM phase [Fig. 2(a)] may be generated by the competition between two terms in Eq. (3) as they have opposite signs and different temperature and field dependencies. In particular, the (positive) AFM order parameter saturates at low temperatures, while the absolute value of the (negative) second term still increases as the square of susceptibility. However, this is only one of the possible reasons for the observed nonlinearity. The second mechanism of the ME effect nonlinearity can be caused by spin-flip and spin-flop transitions, but for PFN the critical fields of these transitions are much higher than those used in our experiment. Namely, the estimations of both the above fields from exchange energies [2,30] show that they are larger than 50 and 250 kOe, respectively. Magnetostriction may also play a role in the AFM phase. As it will be shown in Sec. IV, a simple phenomenological Landau-Ginzburg-Devonshire (LGD) approach with appropriate coefficients in

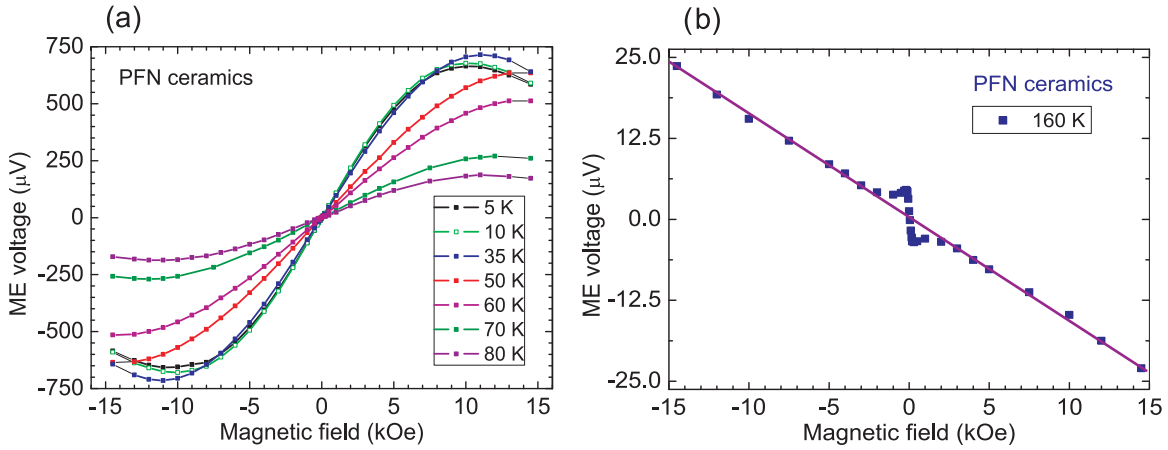

FIG. 2. ME voltage vs magnetic field in AFM (a) and PM (b) phases of PFN ceramics at selected temperatures shown in the legends. The anomaly around zero magnetic field in (b) is due to a parasitic superparamagnetic phase. Solid lines show the fits to Eqs. (33) and (34) of Sec. IV.

the free-energy expansion allows one to explain satisfactorily the ME response nonlinearity.

In the PM phase where $L = 0$, the ME voltage becomes a linear function of the magnetic field [Fig. 2(b)] as only the PM term contributes to the ME effect now. The anomaly around zero magnetic field is produced by a parasitic superparamagnetic phase in ceramics.

B. ME effect in PFN-xPT solid solution

An addition of PT to PFN permits us to manipulate the parameters of magnetic and FE phase transitions in the PFN-xPT solid solution. For instance, at the PT concentration x is larger than about 10 mol %, the long-range AFM ordering of Fe^{3+} spins is suppressed [2,4], and the ferroelectric phase has tetragonal symmetry [4,7]. For the reader's convenience, Fig. 3 reports the magnetic and electric phase diagrams of PFN-xPT

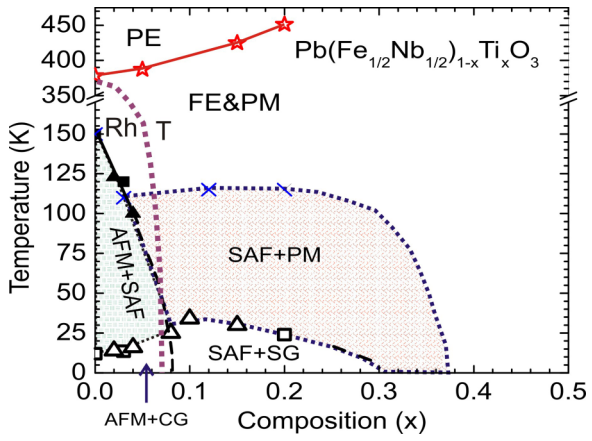

FIG. 3. Phase diagrams of PFN-xPT solid solution. Solid and dashed lines separate different magnetic and electric phases. The red line with stars separates paraelectric (PE) and ferroelectric (FE) phases. The dotted brown line marks the morphotropic phase boundary between rhombohedral (Rh) and tetragonal (T) phases. SAF indicates the superantiferromagnetic state. SG and CG stand for spin-glass and spin-cluster-glass states, respectively [1,2].

solid solution plotted on the base of published experimental data [2,4,7].

Figure 4(a) shows temperature dependence of the ME voltage measured in the PFN-0.03PT crystal. The weak dilution of PFN by nonmagnetic Ti ions lowers the Néel temperature from 150 to 120 K but does not essentially change the temperature behavior of the ME response. The latter becomes much more nonlinear vs the magnetic field as compared to undoped material [Fig. 4(b)]. Both Figs. 4(a) and 4(b) show some anomalous variation in ME response at the temperatures 30–40 K. For instance, the magnetic field dependence of the ME voltage in Fig. 4(b) changes its slope from negative to positive at $H > 13$ kOe. The physical origin of this feature is presently not clear.

It is expected that further increase of the Ti concentration would weaken the AFM phase so that the negative PM-like (i.e., PME) contribution may become dominating. Indeed, the negative PME contribution dominates at all the temperatures already for PFN-0.05PT [Fig. 5(a)] as its Néel temperature is essentially shifted to low temperatures around 55–60 K. Besides, as it can be seen from the phase diagram (Fig. 3), the magnetic state of this composition is complex enough. It contains superposition of various phases: PM, superantiferromagnetic (SAF), AFM, and spin glass (SG). Therefore, a complex interplay between electric and different magnetic order parameters occurs in PFN-0.05PT. As a result, the ME response being a perfect linear function of magnetic field in the PM phase becomes strongly nonlinear at lower temperatures in the magnetically ordered phase even at low fields of a few kOe [Fig. 5(b)]. This composition is also close to the morphotropic boundary between the tetragonal and rhombohedral phases. We cannot thus exclude the rotation of the polarization from the [111] rhombohedral axis to the [100] tetragonal one on cooling that will essentially influence the ME response. At $T \approx 35$ K, the ME coefficient is negative with large enough modulus, $\beta = -1.5 \times 10^{-17}$ s/A. We calculate this value from the slope of the $U_{ME}(H)$ curve at low fields. However, the ME coefficient decreases almost to zero on further cooling even at low fields due to the competition between the AFM phase and spin-glass state.

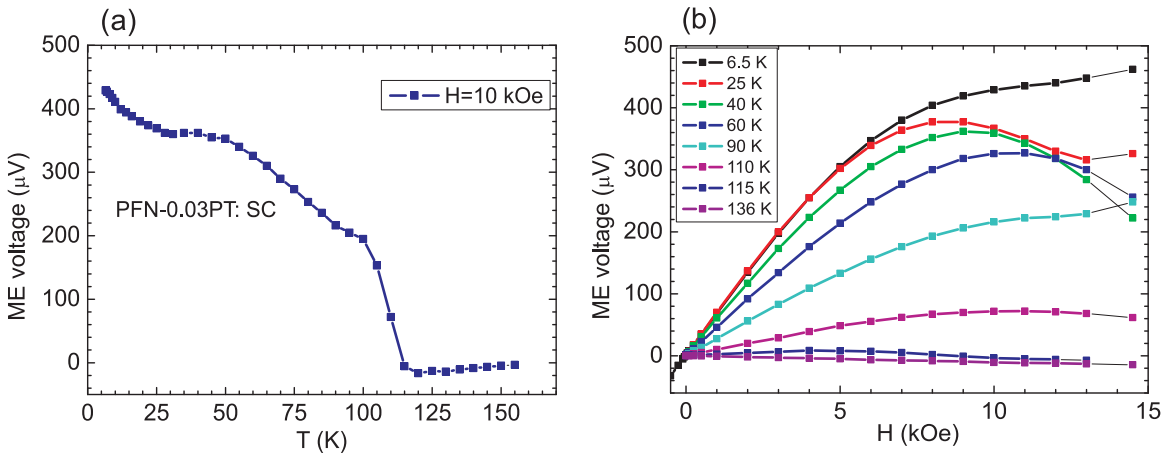

FIG. 4. Temperature (a) and magnetic field (b) dependencies of the ME voltage in PFN-0.03PT solid solution crystal under magnetic field parallel to the [111] crystal direction.

Further dilution of PFN by Ti (PFN-0.2PT composition) suppresses the long-range ordering of Fe^{3+} spins so that only a spin-glass state emerges below the freezing temperature about 23 K. This can be seen from zero field cooled (ZFC) and field cooled (FC) magnetic susceptibilities shown in the inset of Fig. 6(a) and the phase diagram in Fig. 3. The ME voltage thus increases on cooling according to temperature variation of the FC magnetic susceptibility as polarization and dielectric susceptibility are almost constant at these temperatures; see Fig. 6(a). The ME response is negative, PME-like, but large enough at low temperatures ($\beta = -1.45 \times 10^{-17}$ s/A at $T = 10$ K), being comparable with that in the AFM phase of PFN. The ME response is a perfect linear function of applied magnetic field even at the lowest temperatures, Fig. 6(b). The data presented in Fig. 6 can be thus described by the following relation derived by us in Ref. [18]:

$$\beta(T) = -P_S(T)\chi_{\mathrm{FE}}(T)[\chi_M(T)]^2\xi_{MP}. \qquad (4)$$

The solid line in Fig. 6(a) is a fit to Eq. (4) assuming that the only temperature-dependent quantity is the magnetic susceptibility shown in the inset of Fig. 6(a). Taking into account that the FC susceptibility in the SAF and SG phases depends on magnetic field (it was measured at 500 Oe, while ME voltage was measured at 10 kOe), we obtain the qualitatively good coincidence with experiment.

IV. MAGNETOELECTRIC COEFFICIENT IN THE SIMPLE PHENOMENOLOGICAL MODEL

A. Statement of the problem and free-energy function

The electric polarization of a magnetoelectric depends on magnetic field H, $P_{\mathrm{ME}} \equiv P(H)$. Below we will find $P(H)$ from the minimum of corresponding free energy, but for now we suppose that the function $P(H)$ is known. The magnetic field in experiment consists of two parts,

$$H = H_{\mathrm{dc}} + h_{\mathrm{ac}}, \quad h_{\mathrm{ac}} = h\sin\omega t, \quad h_{\mathrm{ac}} \ll H_{\mathrm{dc}}.$$

As $h_{\mathrm{ac}} \ll H_{\mathrm{dc}}$, we can expand the polarization $P(H) = P(H_{\mathrm{dc}} + h_{\mathrm{ac}})$ in a power series in small h_{ac}. This yields

$$P(H_{\mathrm{dc}} + h_{\mathrm{ac}}) \approx P(H_{\mathrm{dc}}) + h_{\mathrm{ac}}\left.\frac{dP}{dH}\right|_{H=H_{\mathrm{dc}}} + \cdots.$$

Now, according to Eq. (1b), $P(H_{\mathrm{dc}})$ is proportional to H_{dc}^2; i.e., rewriting Eq. (1b) in scalar notation, we obtain

$$P(H_{\mathrm{dc}}) = P_0 + \tfrac{1}{2}\beta H_{\mathrm{dc}}^2,$$

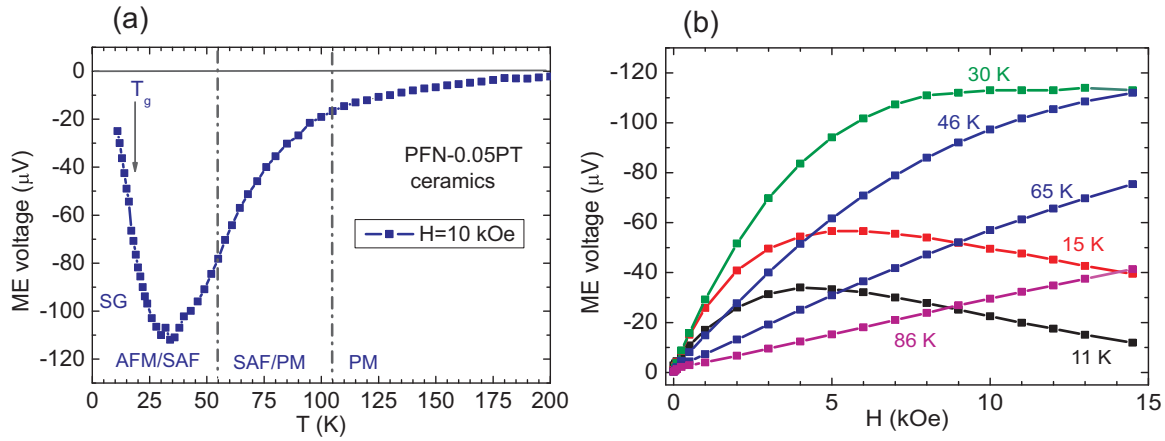

FIG. 5. Temperature (a) and magnetic field (b) dependencies of ME voltage in PFN-0.05PT solid solution ceramics. Vertical dot-dashed lines in (a) separate different magnetic phases.

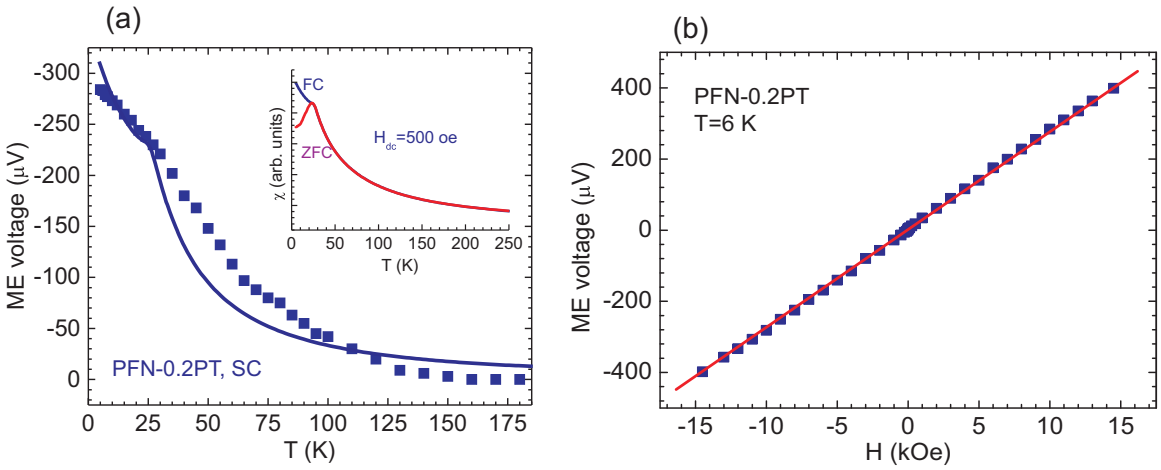

FIG. 6. (a) Temperature dependence of the ME voltage in PFN-0.2PT solid solution crystal measured under the field 10 kOe. The solid line is a fit to Eq. (4) assuming temperature dependence of the only magnetic susceptibility presented in the inset. (b) Magnetic field dependence of the ME voltage at $T = 6$ K.

where P_0 comprises three first terms in Eq. (1b) and β is a quadratic ME coupling coefficient. The term $P(H_{\rm dc})$ is inaccessible by experiment with lock-in detection on the frequency of the $h_{\rm ac}$ field so that we have for experimentally measurable polarization

$$P_{\rm ac}(H) \approx h \left.\frac{dP}{dH}\right|_{H=H_{\rm dc}}.$$

As the measured ME voltage is related to the polarization as $U_{\rm ME} = (S/C)P_{\rm ac}(H)$, where S is an area of electrode and C is a sample capacity, we finally obtain

$$U_{\rm ME} = \frac{S}{C}P_{\rm ac}(H) \approx \frac{Sh}{C}\left.\frac{dP}{dH}\right|_{H=H_{\rm dc}}.$$

As the coefficient Sh/C does not depend on $H = H_{\rm dc}$, i.e., it is a constant, our result for $U_{\rm ME}$ will be proportional to dP/dH. By comparing Eq. (2) with the last expression, the quadratic ME coefficient can be expressed as

$$\beta = \frac{1}{H_{\rm dc}}\frac{dP}{dH}, \quad H = H_{\rm dc}. \tag{5}$$

The aim of the present consideration is to study the magnetic field and temperature dependence of the magnetoelectric coefficient β of $Pb(Fe_{1/2}Nb_{1/2})O_3$ to describe the experiment in its PM and AFM phases. Below we suggest a simple phenomenological approach which can be used not only for a description of the ME effect in PFN, but in other AFM multiferroics. For this purpose we use the simplest possible free-energy function [18]:

$$\begin{aligned} G &= G_P + G_M + G_{\rm ME}, \\ G_P &= \tfrac{1}{2}\alpha_P(T)P^2 + \tfrac{1}{4}\beta_P P^4 - PE, \\ G_{\rm ME} &= \tfrac{1}{2}\left(\xi_{MP}M^2 + \xi_{LP}L^2\right)P^2, \\ G_M &= \tfrac{1}{2}\alpha_L(T)L^2 + \tfrac{1}{4}\beta_L L^4 + \tfrac{1}{2}\alpha_M(T)M^2 \\ &\quad + \tfrac{1}{4}\beta_M M^4 + \tfrac{1}{2}\xi_{LM}L^2M^2 - MH, \end{aligned} \tag{6}$$

where P, M, and L are, respectively, ferroelectric (polarization), ferromagnetic (magnetization), and AFM order parameters; E and H are the strengths of external electric and magnetic fields. The only temperature-dependent coefficients are those where explicit temperature dependence is indicated, namely,

$$\begin{aligned} &\alpha_P(T) = \alpha_{P_0}(T - T_C), \quad \alpha_M(T) = \alpha_{M_0}(T - \theta), \\ &\alpha_L(T) = \alpha_{L_0}(T - T_N), \end{aligned} \tag{7}$$

where $T_C \approx 370$ K is the temperature of paraelectric-ferroelectric phase transition, $T_{\rm N} \approx 150$ K is the Néel temperature, and $\theta \approx -520$ K is the temperature of the (virtual) ferromagnetic phase transition [2]. Below we will use this phase transition temperature hierarchy to describe the experimentally observed $\beta(T, H)$ dependencies. Note that for our purposes it is sufficient to consider the ferroelectric phase transition of the second kind; i.e., we truncate the power series in G_P on the P^4 term assuming that $\beta_P > 0$.

We note here that the stresses and strains are already included implicitly in the free-energy function (6). The point is that for the quasihomogeneous system (single crystal, poled micrograin ceramics) studied here, the inhomogeneous stresses are effectively averaged so that only spatially homogeneous ones can affect the free energy. In turn, the homogeneous spontaneous elastic stresses and strains can be "removed" from the resulting free-energy function (6) by the preceding minimization of the initial free-energy function over stresses and strains. This had been done in Ref. [31] and leads simply to renormalization of the initial free-energy function coefficients.

B. Calculation of temperature and magnetic field dependence of magnetoelectric coefficient

The idea behind this calculation is natural and simple. First, minimizing the free energy (6), we find the field (magnetic and electric) and temperature dependences of order parameters P, M, and L and then, taking the derivative dP/dH (with respect to the field and temperature dependences of the rest order parameters), obtain the desired dependence $\beta(T,H)$ in paramagnetic ($L = 0, T > T_N$) and antiferromagnetic ($L \neq 0, T < T_N$) phases of PFN. Note that according

to Eq. (5) the quadratic ME coefficient can be expressed as $\beta = (1/H)(dP/dH)$. Therefore, the experimentally measured ME voltage is directly proportional to the dP/dH.

The equations for equilibrium order parameters assume the form

$$\frac{\partial G}{\partial P} = 0, \quad \frac{\partial G}{\partial M} = 0, \quad \frac{\partial G}{\partial L} = 0, \tag{8}$$

$$\frac{\partial G}{\partial P} = P(\alpha_P + \xi_{MP}M^2 + \xi_{LP}L^2) + \beta_P P^3 - E = 0, \tag{9}$$

$$\frac{\partial G}{\partial M} = M(\alpha_M + \xi_{LM}L^2 + \xi_{MP}P^2) + \beta_M M^3 - H = 0, \tag{10}$$

$$\frac{\partial G}{\partial L} = L(\alpha_L + \xi_{LM}M^2 + \xi_{LP}P^2) + \beta_L L^2. \tag{11}$$

We pay attention here that as parameters P and M couple with external fields [there are terms PE and MH in the free energy (6) and hence E and H in Eqs. (9) and (10)], while L does not, this permits us to factor Eq. (11) for L considering separately the cases $L = 0$ (PM phase) and $L \neq 0$ (AFM phase). This eventually yields the nonlinear dependence $\beta(H)$ in the AFM phase.

Actually, the set of equations (8) [with respect to its detailed versions (9)–(11)] contains all the information we need. Namely, it determines the fields (electric and magnetic) and temperature dependences of order parameters P, M, and L and hence their field (and temperature if necessary) derivatives also.

The set (9)–(11) has plenty of solutions depending on the phase we choose. The experiment to be described suggests to us what class of solutions we are to pick up. Namely, as we do not have experimental dependences on the electric field, we set it to be zero: $E = 0$. The second fact is that ferroelectric $T_C = 370$ K is higher then $T_N = 150$ K so that the spontaneous polarization P exists and we do not choose the solution $P = 0$ (at $E = 0$) of Eq. (9). Rather, we cancel P in (9) at $E = 0$ and obtain the following equation for spontaneous polarization $P = P(T,H)$:

$$\alpha_P + \xi_{MP}M^2 + \xi_{LP}L^2 + \beta_P P^2 = 0. \tag{12}$$

The set of equations (12), (10), and (11) defines the necessary solutions for our experimental case of interest. Namely, in the paramagnetic case we should consider solutions with $L = 0$ while in AFM one we consider $L \neq 0$.

1. *Paramagnetic phase*

In the paramagnetic phase we consider the solution $L = 0$ so that Eq. (11) is satisfied identically. The set of remaining equations at $L = 0$ assumes the form

$$\alpha_P + \xi_{MP}M^2 + \beta_P P^2 = 0, \tag{13}$$

$$M(\alpha_M + \xi_{MP}P^2) + \beta_M M^3 = H. \tag{14}$$

Note that while here P is spontaneous (electric-field-independent) polarization, the magnetization M is entirely generated by magnetic field. In principle, the nonlinear term $\beta_M M^3$ can be neglected but we will not do that as the set (13) and (14) is very simple and admits an analytical expression for magnetoelectric coefficient. Namely, it follows from Eq. (13) that

$$P^2 = \frac{-\alpha_P - \xi_{MP}M^2}{\beta_P} \Rightarrow P = P_s(T)\sqrt{1 - \frac{\xi_{MP}M^2}{|\alpha_P(T)|}}, \tag{15}$$

where we explicitly show the temperature-dependent quantities. Here $P_s^2 = -\alpha_P/\beta_P > 0$ is a spontaneous polarization value in the "pure ferroelectric" (i.e., without magnetic contribution) case, where $\alpha_P < 0$. The derivative dP/dH can be easily obtained from (15)

$$U_{\mathrm{ME}} \sim \frac{dP}{dH} = -\frac{P_s(T)\xi_{MP}}{\left|\alpha_P(T)\sqrt{1 - \frac{\xi_{MP}M^2}{|\alpha_P(T)|}}\right|} M\frac{dM}{dH}$$

$$\equiv -\frac{\xi_{MP}}{\sqrt{\beta_P}\sqrt{|\alpha_P(T)| - \xi_{MP}M^2}} M\frac{dM}{dH}. \tag{16}$$

The last expression in (16) shows that the temperature dependence of $\beta \sim dP/dH$ in paramagnetic phase comes from $|\alpha_P(T)|$ under the square root in the denominator and hence is weak. Another important fact is that we already have a negative sign of β. This is because $\xi_{MP} > 0$ (at least this can be asserted from comparison with experiment) and $MM' = (1/2)(dM^2/dH) > 0$ as $M(H)$ is an increasing function.

The dependence $M(H)$ can be obtained from (10) by substitution of P^2 from Eq. (15), which yields

$$Q_1 M + Q_2 M^3 = H, \quad Q_1 = \alpha_M(T) + \frac{|\alpha_P(T)|\xi_{MP}}{\beta_P},$$

$$Q_2 = \beta_M - \frac{\xi_{MP}^2}{\beta_P}. \tag{17}$$

In this case

$$\frac{dM}{dH} = \frac{1}{Q_1 + 3Q_2M(H)^2}. \tag{18}$$

To find the dependence $U_{\mathrm{ME}}(H,T) \sim dP/dH$ numerically, we first solve Eq. (17) at a given temperature for $M(H)$ and then substitute the obtained solution to Eq. (16) with respect to relation (18). Our numerical solution shows (see also below) that the dependence $U_{\mathrm{ME}}(H,T)$ is a linear function of H and in the experimentally available temperature range ($\sim$150−200 K) it is almost temperature independent.

To obtain $U_{\mathrm{ME}}(H,T)$ analytically, we look for a solution of Eq. (17) in the form

$$M = \chi_1 H + \chi_3 H^3 + \cdots + \chi_{2n+1}H^{2n+1}. \tag{19}$$

Substitution of this expression into Eq. (16) gives for the first two coefficients (we can calculate as many coefficients as possible) $\chi_1 = 1/Q_1$, $\chi_3 = -Q_2/Q_1^4$ so that

$$M \approx \frac{H}{Q_1} - \frac{Q_2}{Q_1^4}H^3. \tag{20}$$

Then, in the lowest approximation in H,

$$P \approx P_s\left(1 - \frac{1}{2}\frac{\xi_{MP}H^2}{Q_1^2|\alpha_P|}\right), \tag{21}$$

$$U_{\mathrm{ME}} \sim \frac{dP}{dH} = -\frac{\xi_{MP}}{Q_1^2\sqrt{|\alpha_P|\beta_P}}H. \tag{22}$$

The expression (22) is the solution in the paramagnetic phase. In accord with experiment it has the form of a linear function of H with a negative slope. Below we will rewrite its temperature dependence explicitly and plot this dependence.

2. *Antiferromagnetic phase*

Although this case is more complicated than the paramagnetic one, the method of solution here is essentially the same. In this case we consider the solution with $L \neq 0$ (spontaneous AFM moment) of Eq. (11). Canceling L in (11), we obtain now the following system of equations instead of (13) and (14):

$$\alpha_L + \xi_{LM} M^2 + \xi_{LP} P^2 + \beta_L L^2 = 0, \tag{23}$$

$$M(\alpha_M + \xi_{LM} L^2 + \xi_{MP} P^2) + \beta_M M^3 = H. \tag{24}$$

Equations (12), (23), and (24) constitute the "master" set of equations for the AFM phase. Equation (23) permits us to express L^2 via M^2 and P^2 and eliminate it from (24). This yields

$$M\left[\alpha_M + \xi_{LM} L_0^2 + P^2\left(\xi_{MP} - \frac{\xi_{LM}\xi_{LP}}{\beta_L}\right)\right] + M^3\left(\beta_M - \frac{\xi_{LM}^2}{\beta_L}\right) = H. \tag{25}$$

Here we introduce the equilibrium spontaneous AFM moment $L_0^2 = -\alpha_L/\beta_L$. The next step is to use the same trick to eliminate L^2 from Eq. (12) thus expressing P^2 via M^2 only. We have

$$\begin{aligned} P^2 &= P_s^2 - \frac{\xi_{MP}}{\beta_P} M^2 - \frac{\xi_{LP}}{\beta_P} L^2 = P_s^2 - \frac{\xi_{MP}}{\beta_P} M^2 \\ &\quad - \frac{\xi_{LP}}{\beta_P}\left(L_0^2 - \frac{\xi_{LM}}{\beta_L} M^2 - \frac{\xi_{LP}}{\beta_L} P^2\right) \\ &= P_s^2 - \frac{\xi_{LP}}{\beta_P} L_0^2 - M^2\left(\frac{\xi_{MP}}{\beta_P} + \frac{\xi_{LM}}{\beta_L}\right) + \frac{\xi_{LP}^2}{\beta_P \beta_L} P^2. \end{aligned} \tag{26}$$

Equation (26) for P^2 looks complicated but actually it has a simple form, $P^2 = a_1 + a_2 P^2$. Its solution has the form $P^2 = a_1/(1 - a_2)$, or explicitly,

$$\begin{aligned} P^2 &= A_0 + B_0 M^2, \quad A_0 = \frac{P_s^2 - \frac{\xi_{LP}}{\beta_P} L_0^2}{1 - \frac{\xi_{LP}^2}{\beta_P \beta_L}}, \\ B_0 &= \frac{1}{\beta_P} \frac{\frac{\xi_{LM}\xi_{LP}}{\beta_L} - \xi_{MP}}{1 - \frac{\xi_{LP}^2}{\beta_P \beta_L}}. \end{aligned} \tag{27}$$

Substitution of Eq. (27) into Eq. (25) generates the following equation for $M(H)$:

$$U_1 M + U_2 M^3 = H, \tag{28}$$

$$U_1 = \alpha_M + \xi_{LM} L_0^2 + A_0\left(\xi_{MP} - \frac{\xi_{LM}\xi_{LP}}{\beta_L}\right),$$

$$U_2 = \beta_M - \frac{\xi_{LM}^2}{\beta_L} + B_0\left(\xi_{MP} - \frac{\xi_{LM}\xi_{LP}}{\beta_L}\right).$$

Equation (28) has a form similar to Eq. (17). To obtain coefficients Q_1 and Q_2, we should not only put $L_0 = 0$ in U_1 and U_2 but also put $\xi_{LM} = \xi_{LP} = 0$. The comparison of $P^2(M^2)$ dependences in the PM phase (15) and in the AFM phase (27) shows that while in the AFM phase $B_0 > 0$, in the PM phase ($\xi_{LM} = \xi_{LP} = 0$) B_0 becomes negative which is responsible for the sign change of magnetoelectric coefficient while traversing T_N.

Proceeding along the same lines, as in the PM phase, we obtain the desired dependence $\beta(T,H)$ in the AFM phase, suitable for numerical calculations,

$$\begin{aligned} U_{\mathrm{ME}} \sim \frac{dP}{dH} &= \frac{B_0}{\sqrt{A_0 + B_0 M^2}} M \frac{dM}{dH}, \\ \frac{dM}{dH} &= \frac{1}{U_1 + 3M^2 U_2}. \end{aligned} \tag{29}$$

The numerical calculations with the help of Eq. (29) show that it is possible to obtain very good analytical approximation to this expression. Namely, looking for an approximate solution of Eq. (28) in the form (19), we obtain

$$M \approx \frac{H}{U_1} - \frac{U_2}{U_1^4} H^3, \tag{30}$$

and further substitute this solution into (29). This gives the analytical formula, whose numerical outcome is indistinguishable from that of (29):

$$\frac{dP}{dH} = \frac{B_0 H}{U_1^2} \frac{\frac{1}{U_1} - \frac{4U_2}{U_1^4} 1 H^2}{\sqrt{A_0 + \frac{B_0}{U_1^2} H^2 - \frac{2B_0 U_2}{U_1^5} H^4}}. \tag{31}$$

The approximate analytical solution in the form of a power series gives

$$\begin{aligned} \frac{dP}{dH} &\approx \frac{B_0 H}{U_1^2 \sqrt{A_0}}\left[1 - H^2 \frac{U_1 B_0 + 8 U_2 A_0}{2 A_0 U_1^3}\right], \\ \beta = \frac{1}{H}\frac{dP}{dH} &\approx \frac{B_0}{U_1^2 \sqrt{A_0}}\left[1 - H^2 \frac{U_1 B_0 + 8 U_2 A_0}{2 A_0 U_1^3}\right], \end{aligned} \tag{32}$$

showing explicitly that the ME coefficient β is positive for low fields but it decreases with field increase.

C. Numerical results

1. *Theoretical curves*

It is convenient to introduce the dimensionless temperature $\tau = T/T_C$ and coefficient $\kappa = T_C/T_N > 1$. As in PFN $T_C \approx 370\,\mathrm{K}, T_N \approx 150\,\mathrm{K}$, and $\theta \approx -520\,\mathrm{K}$, in these units the ferroelectric phase is realized at $\tau < 1$ and AFM phase at $\tau < 1/\kappa = 15/37 \approx 0.405$. Hence the PM phase occurs at $0.405 < \tau < 1$. Now we rewrite the temperature-dependent

coefficients in the above units to obtain

$$A_0 = \frac{\alpha_{P_0} T_C}{\beta_P\left[1 - \frac{\xi_{LP}^2}{\beta_P \beta_L}\right]}[1 - \tau - \kappa_2(1 - \kappa\tau)] \equiv a_1 + a_2\tau,$$

$$a_1 = \frac{\alpha_{P_0} T_C}{\beta_P\left[1 - \frac{\xi_{LP}^2}{\beta_P \beta_L}\right]}(1 - \kappa_2), \quad a_2 = \frac{\alpha_{P_0} T_C}{\beta_P\left[1 - \frac{\xi_{LP}^2}{\beta_P \beta_L}\right]}(\kappa_2\kappa - 1), \quad \kappa_2 = \frac{\xi_{LP}\alpha_{L_0} T_N}{\beta_L \alpha_{P_0} T_C}. \tag{33}$$

$$Q_1 = \alpha_{M_0} T_C\left(\tau + \frac{|\theta|}{T_C}\right) + \frac{\xi_{MP}\alpha_{P_0} T_C}{\beta_P}(1 - \tau) \equiv q_{11} + q_{12}\tau, \ \sqrt{|\alpha_P|} = q_{13}\sqrt{1 - \tau}, \tag{34}$$

$$q_{11} = \alpha_{M_0}|\theta| + \frac{\xi_{MP}\alpha_{P_0} T_C}{\beta_P}, \ q_{12} = \alpha_{M_0} T_C - \frac{\xi_{MP}\alpha_{P_0} T_C}{\beta_P}, \ q_{13} = \sqrt{\alpha_{P_0} T_C}.$$

$$U_1 = g_1\left(\tau + \frac{|\theta|}{T_C}\right) + g_2(1 - \kappa\tau) + g_3[1 - \tau - \kappa_2(1 - \kappa\tau)] \equiv u_{11} + u_{12}\tau, \tag{35}$$

$$g_1 = \alpha_{M_0} T_C, \ g_2 = \frac{\xi_{LM}\alpha_{L_0} T_N}{\beta_L}, \ g_3 = \frac{\alpha_{P_0} T_C}{\beta_P\left[1 - \frac{\xi_{LP}^2}{\beta_P \beta_L}\right]}\left(\xi_{MP} - \frac{\xi_{LM}\xi_{LP}}{\beta_L}\right),$$

$$u_{11} = g_1\frac{|\theta|}{T_C} + g_2 + g_3(1 - \kappa_2), \ u_{12} = g_1 - g_2\kappa + g_3(\kappa_2\kappa - 1).$$

The reduced temperatures are equal to $|\theta|/T_C \equiv 520/370 = 1.405$, $\kappa = T_C/T_N = 2.47$. Having temperature-dependent parameters (33)–(35), we can write the dependences $U_{\rm ME}(H,\tau)$ in both PM and AFM phases explicitly,

$$U_{\rm ME} \sim \frac{dP}{dH} = -p_0\frac{H}{(q_{11} + q_{12}\tau)^2\sqrt{1 - \tau}}, \ p_0 = \frac{\xi_{MP}}{q_{13}\sqrt{\beta_P}}, \quad \text{PM} \quad \text{phase}, \tag{36}$$

$$U_{\rm ME} \sim \frac{B_0 H}{(u_{11} + u_{12}\tau)^{5/2}}\frac{(u_{11} + u_{12}\tau)^3 - 4U_2 H^2}{\sqrt{(a_1 + a_2\tau)(u_{11} + u_{12}\tau)^5 + B_0(u_{11} + u_{12}\tau)^3 H^2 - 2B_0 U_2 H^4}}, \quad \text{AFM} \quad \text{phase}, \tag{37}$$

where B_0 and U_2 are also (fitting) parameters. Note that magnetic field H here can be regarded as both a dimensional and a dimensionless quantity. Really, if we divide H by some H_0 and introduce dimensionless field $h = H/H_0$, we simply renormalize coefficients such as p_0.

The field dependences (36) and (37) are reported in Fig. 7. The close resemblance to corresponding experimental curves can be seen. Below we will fit these curves to real experimental data.

We plot the temperature dependence of ME voltage in Fig. 8 at dimensionless magnetic field $h = 1$ and other parameters similar to those in Fig. 7. At $T = T_N$ the discontinuity in the temperature dependence is seen. This discontinuity is due to the fact that coefficients ξ_{LM} and ξ_{LP} do not have temperature dependence and appear abruptly in the AFM phase. In our opinion, the effects of weak site disorder in the Fe spins of PFN would, in accordance with experiment, lift this discontinuity. These effects give spin-glass features such as the difference in field cooled and field heated regimes, which are present in the vicinity of T_N in the experimental curves. The smearing of the discontinuity may appear in the form of additional temperature dependence of the coefficients ξ_{LM} and ξ_{LP} so that they will no more appear abruptly in AFM phase.

2. *Fitting to experiment*

The fitting of the field dependences of the ME voltage by the expressions (33) (PM phase) and (34) (AFM phase) is shown in Fig. 2 by solid lines. The best fit in the AFM phase [Fig. 2(a)] has been achieved for the following parameters values: $B_0 = 1000, U_2 = 0.04, u_{11} = 0.9, u_{12} = 0.376, a_1 = 1.0, a_2 = 2.9933$. For Fig. 2(b) (PM phase) the best fit is achieved at $q_{11} = 3.0, q_{12} = 2.2, p_0 = 185.85$. We note that the latter sets of best fit parameters are

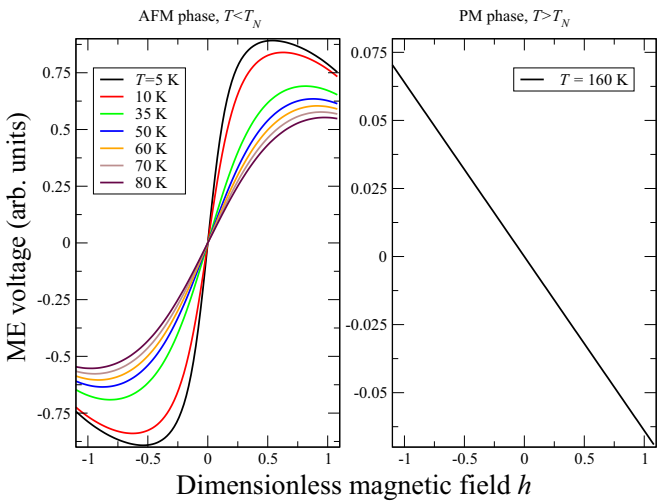

FIG. 7. Magnetic field dependence of ME voltage (arbitrary units) in AFM (left panel) and PM (right panel) phases at different temperatures, shown in the legend. The curves have been plotted using Eqs. (36) and (37) with the following parameters: $B_0 = 0.6, U_2 = 0.04, u_{11} = 0.762162, u_{12} = 0.376, a_1 = 0.01, a_2 = 2.9333$.

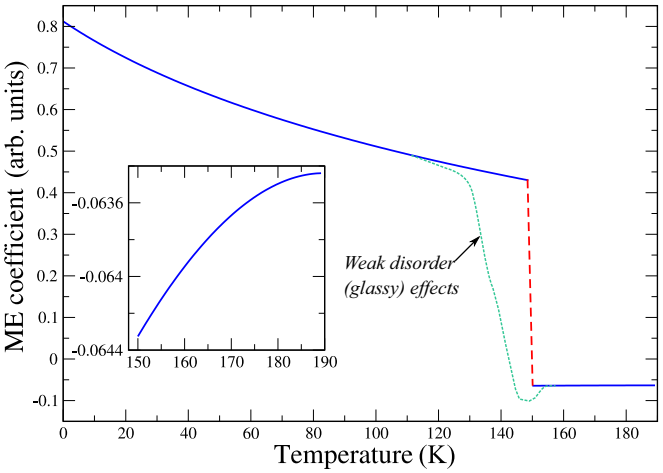

FIG. 8. Temperature dependence of ME coefficient (arbitrary units) at dimensionless magnetic field $h = 1$. The parameters are similar to those used in Fig. 7. At $T = T_N$ the discontinuity in the temperature dependence is seen. This discontinuity is attributed to the fact that the coefficients ξ_{LM} and ξ_{LP} do not depend on temperature and appear abruptly in the AFM phase. The effects of weak disorder in the Fe spins in PFN lead to spin-glass effects which smear the discontinuity at $T = T_N$. The inset highlights the temperature dependence in the PM phase at $T > T_N = 150$ K.

not unique so that additional experiments may be required to determine unambiguously the coefficients of phenomenological free-energy function (6) and hence the above parameters. Nevertheless, the excellent coincidence with experimental data is well seen. In our view this is because the simple phenomenological approach, although having many unknown coefficients, accounts correctly for order parameters coupling with magnetic (and electric) fields.

At the same time, visual comparison of theoretical curve $U_{\rm ME}(T)$ at fixed H in both phases and experimental ones shows that it is barely possible to achieve the quantitative coincidence between theory and experiment in this case. Our analysis confirms this point as we were not able to find a suitable set of parameters which permits us to achieve the slope of the $U_{\rm ME}(T)$ curves observed in experiment at low temperatures. This is because the phenomenological LGD approaches usually have simplified temperature dependences of their coefficients, which do not account, e.g., for possible spin-glass effects. Hence, although it is possible to achieve excellent quantitative coincidence in the $U_{\rm ME}$ field dependences, the temperature dependences can be described only qualitatively. For quantitative description of the temperature dependence, more sophisticated approaches, considering (weak) disorder effects, should be utilized.

V. DISCUSSION

We determined the quadratic ME coefficients for PFN and its solid solutions with PT and listed them in Table I. This table compares our values with the literature data for some other magnetoelectric materials. In particular, the ME coefficient is approximately the same in the PM phase of PFN and PFN-PT as in the paramagnetic $Gd_2(MoO_4)_3$ and $NiSO_4 \cdot 6H_2O$ single crystals. In the AFM phase of PFN and PFN-PT, it increases by almost two orders of magnitude exhibiting sign reversal at the AFM phase transition. ME coefficient values for PFN and PFN-PT are two to three orders of magnitude higher than those for the well-known multiferroic $BiFeO_3$ and magnetoelectrics $CsCuCl_3$, $Ni_3B_7O_{13}Cl$, and $BaMnF_4$ with weak ferroelectricity. Note that although the ME effect is weak in $ScCuCl_3$, it shows the sign reversal at the AFM phase transition similar to PFN [33].

Another important fact to which we want to draw attention is the strong nonlinearity of the ME effect in the AFM phase of PFN and PFN-PT even at low fields, 5–15 kOe. Usually nonlinearity of the ME effect appears in the vicinity of spin-flip, spin-flop, or other magnetic field induced phase transitions. The phenomenological theory introduced in Sec. IV allows one to describe this nonlinearity by choosing appropriate values for coefficients of the free-energy expansion. Obviously, the most important is the coefficient ξ_{LP}, which describes the coupling of ferroelectric polarization to AFM order parameter. This coefficient cannot be directly extracted from our experiment.

TABLE I. Quadratic β_{333} ME coefficients in paramagnetic, antiferromagnetic, and spin-glass phases of PFN and PFN-PT solid solutions. SC stands for single crystal. For comparison, the measured quadratic ME coefficient is reported for other AFM magnetoelectrics.

Material	PM phase	AFM phase	SG phase	References
PFN, SC		2.5×10^{-17} s/A		This paper
PFN, SC		$(1-10) \times 10^{-17}$ s/A		[17,1]
PFN, ceramics	-1×10^{-18} s/A	9.6×10^{-17} s/A		This paper
PFN-0.03PT, SC		4.8×10^{-17} s/A		This paper
PFN-0.05PT ceramics	-2×10^{-18} s/A		-1.5×10^{-17} s/A	This paper
PFN-0.2PT, SC			-1.45×10^{-17} s/A	This paper
$BiFeO_3$, SC		2.1×10^{-19} s/A		[19,20]
$Gd_2(MoO_4)_3$, SC	0.8×10^{-18} s/A			[32]
$NiSO_4 \times 6H_2O$, SC	2.2×10^{-9}esu			[26]
	0.7×10^{-18} s/A			
$CsCuCl_3$, SC	-0.02 pC/(cmT)^2	0.14 pC/(cmT)^2		[33]
	-3.1×10^{-22} s/A	2.2×10^{-21} s/A		
$Ni_3B_7O_{13}Cl$, SC		$\lvert 0.6-1.6\rvert \times 10^{-18}$ s/A		[34]
$BaMnF_4$, SC		$(0.8-1.6) \times 10^{-19}$ s/A		[35]

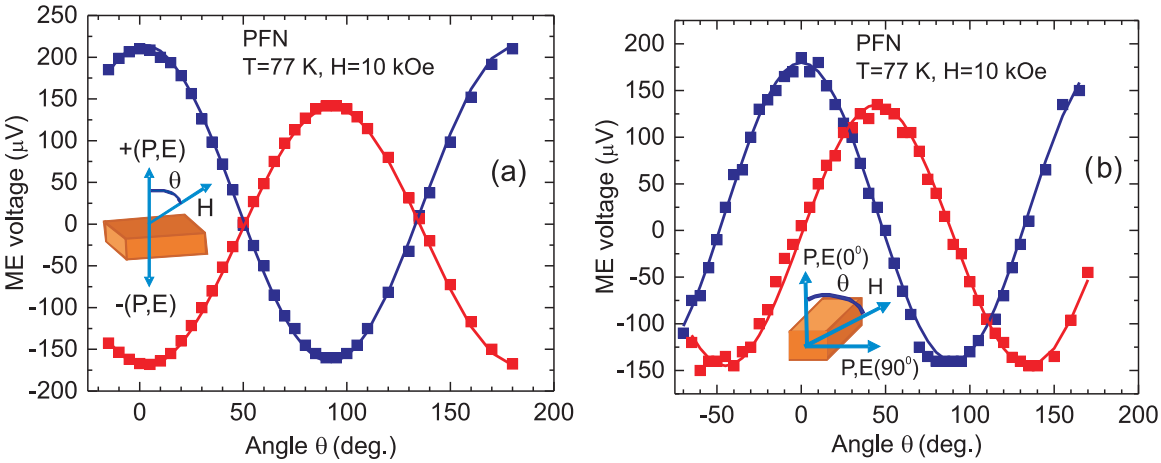

FIG. 9. Angular dependencies of the ME voltage in PFN ceramics under the electric-field polarity reversal (a) and 90° switching of polarization (b) in the AFM phase at $T = 77$ K and $H = 10$ kOe. Solid lines are fit to Eq. (38).

However, it has to be much larger in PFN than in the other magnetoelectrics listed in Table I.

In spite of the fact that the ME effect is highly anisotropic (the quadratic ME coefficient is described by a third-rank tensor) and should be averaged in ceramics, we found approximately the same values of the ME coupling coefficient in both single-crystal and ceramic samples. This means that the magnetic anisotropy generates strong coupling of magnetic domain structure to electric polarization and ferroelectric domains. In other words, for instance, AFM domains can be aligned by external electric field similar to ferroelectric domains. This has been demonstrated previously for $BiFeO_3$ crystals [21]. Therefore, from the application point of view, PFN-based multiferroics are attractive in ME memory elements and spintronics as AFM domains are very stable with respect to external magnetic fields.

Figure 9(a) illustrates the variation of the ME response angular dependence in the AFM phase of PFN ceramics after electric-field polarity reversal with respect to the initial polarization direction. One can see that the ME signal changes sign at electric-field polarity reversal indicating 180° switching of polarization. Both curves are well fitted by the function

$$U_{\mathrm{ME}} = A + B\cos(2\theta - \varphi), \tag{38}$$

where θ is the angle between electric polarization and magnetic field and $\varphi = 0^\circ$ or 180° determines the electric-field polarity. This demonstrates that the ME coefficient (proportional to $B\cos\varphi$) changes sign at the electric-field polarity reversal.

The above experiment does not permit us to discern the influence of the above polarization switching on the AFM order parameter L. This is because the ME response is proportional to L^2 and both lattice distortion and magnetic anisotropy remain to be along the same crystal direction. Here we assume that magnetization and polarization are parallel to each other in accordance with the neutron diffraction data [36] and ME measurements in single crystals [14,17]. However, if the polarization is switched by 71° from the initial rhombohedral direction into an equivalent one (in ceramics, the average polarization switches by 90°), the AFM order parameter should also change its orientation. This occurs due to the influence of magnetic anisotropy, which forces the magnetization to rotate along the polarization direction in order to minimize the lattice energy with respect to a new rhombohedral distortion. Such 90° switching of the polarization in the AFM phase of the ceramic sample is demonstrated in Fig. 9(b), which shows the change of ME voltage angular dependence under the electric-field application perpendicular to the initial polarization direction. One can see that two curves having approximately the same amplitude are now shifted from each other by the angle $\varphi = 90^\circ$, which is two times smaller than in the case of 180° switching of polarization. These data demonstrate that the AFM order parameter L also rotates parallel to electric polarization in the case of 90° switching. In the opposite situation, when the magnetic order parameter retains the initial direction, the two curves in Fig. 9(b) should be essentially different as P and L are coupled by different ME coefficients corresponding to $P||L$ or $P\perp L$. Certainly, in the course of sample cooling from PM to AFM phase under poling field, magnetic domains become aligned. Our results show that both ferroelectric and AFM domains can be directly switched by an electric field also in the AFM phase though the coercive field increases by almost ten times ($E_c \approx 25$ kV/cm) as compared to that in the PM phase [7,18]. To confirm our latter conclusion, additional neutron diffraction or AFM resonance measurements can be used to monitor the AFM domains' rotation. However, the fact that even in ceramics we detect approximately the same strong ME signal at different electric polarization directions suggests that the electric domains' alignment really causes a corresponding adjustment of magnetic domains and this process can be controlled by electric field in the AFM phase.

VI. CONCLUSIONS

To summarize, we have measured ME effect in PFN and PFN-PT solid solutions multiferroics. We perform our measurements both on crystalline and ceramic samples in a broad temperature range from liquid helium up to room temperature. Surprisingly, the ME effect turns out to be approximately the same or even higher in ceramics than in single crystals. In our opinion this is due to the better possibility of poling the ceramics as the resistivity is much

higher. This suggests that the alignment of polar domains leads to corresponding adjustment of magnetic domains as the magnetization axis is coupled to the polarization direction via magnetic anisotropy. The latter anisotropy is high in PFN due to strong lattice distortions generated by ferroelectric phase transition. We also demonstrate the possibility of AFM domains switching by external electric field even in ceramic PFN samples. The latter effect could be attractive for spintronic and ME random access memory applications as ME coupling offers an elegant method of electric-field control and switching of AFM domains. It is worth noting that though the Néel temperature of PFN ($\approx$150 K) is well below room temperature, it can be increased substantially by mechanical activation of precursors used for ceramics sintering [15] and by strain engineering in epitaxial nanofilms [11,37].

There is a sign reversal of the ME coefficient at the paramagnetic-to-antiferromagnetic phase transition. It indicates that the ME response related to the AFM order parameter has the sign opposite to that in the paramagnetic phase. The PM-like contribution is nonzero in the AFM phase in spite of the fact that Fe^{3+} spins are antiferromagnetically ordered. This contribution increases on cooling proportionally to the increase of FC susceptibility. This fact strongly supports the model of the PFN ground magnetic state as coexistence of the long-range ordered AFM phase with the short-range ordered SG state on a microscopic level (see, e.g., Refs. [3,8]). On the other hand, the ME coefficient does not show the sign reversal at the transition from the paramagnetic phase to the spin-glass state. The ME coefficient is negative in both PM and SG states. Note that the ME coefficient in PFN and PFN-PT is almost three orders of magnitude larger than that in $BiFeO_3$. It is obviously related to the fact that L^2P^2 ME coupling is essentially averaged by spin rotations along the $BiFeO_3$ cycloid so that the M^2P^2 term [Eqs. (3) and (6)] contributes primarily to ME response similar to the PM-FE phase of PFN.

While the ME response is a perfect linear function of applied magnetic field in both PM and SG phases, it becomes strongly nonlinear in the AFM phase even at low magnetic fields of only a few kOe. We naturally explain this phenomenon in the framework of Landau theory by choosing appropriate values for coefficients of the free-energy expansion.

ACKNOWLEDGMENTS

The research was supported by the Czech Science Foundation, Project No. 13-11473S, by the Czech Ministry of Education, Youth and Sports, Projects No. LM2015088 and No. LO1409, and partially by the Ministry of Education and Science of Russian Federation through research project 3.1649.2017/PP.

[1] W. Kleemann, V. V. Shvartsman, P. Borisov, and A. Kania, Phys. Rev. Lett. **105**, 257202 (2010).
[2] V. V. Laguta, M. D. Glinchuk, M. Maryško, R. O. Kuzian, S. A. Prosandeev, S. I. Raevskaya, V. G. Smotrakov, V. V. Eremkin, and I. P. Raevski, Phys. Rev. B **87**, 064403 (2013).
[3] S. Chillal, M. Thede, F. J. Litterst, S. N. Gvasaliya, T. A. Shaplygina, S. G. Lushnikov, and A. Zheludev, Phys. Rev. B **87**, 220403(R) (2013).
[4] S. P. Singh, S. M. Yusuf, S. Yoon, S. Baik, N. Shin, and D. Pandey, Acta Mater. **58**, 5381 (2010).
[5] D. A. Sanches, N. Ortega, A. Kumar, G. Sreenivasulu, R. S. Katiyar, J. F. Scott, D. M. Evans, M. Arredondo-Arechavala, A. Schilling, and J. M. Gregg, J. Appl. Phys. **113**, 074105 (2013).
[6] I. P. Raevski, S. P. Kubrin, S. I. Raevskaya, S. A. Prosandeev, M. A. Malitskaya, V. V Titov, D. A. Sarychev, A. V. Blazhevich, and I. N. Zakharchenko, IEEE Trans. Ultrason. Ferroelect. Freq. Control **59**, 1872 (2012).
[7] E. I. Sitalo, I. P. Raevski, A. G. Lutokhin, A. V. Blazhevich, S. P. Kubrin, S. I. Raevskaya, Y. N. Zakharov, M. A. Malitskaya, V. V. Titov, and I. N. Zakharchenko, IEEE Trans. Ultrason. Ferroelect. Freq. Control **58**, 1914 (2011).
[8] V. A. Stephanovich and V. V. Laguta, Phys. Chem. Chem. Phys. **18**, 7229 (2016).
[9] B. Fraygola, N. Frizon, W. J. Nascimento, A. A. Coelho, D. Garcia, and J. A. Eiras, Ferroelectrics **470**, 221 (2014).
[10] R. Blinc, P. Cevc, A. Zorko, J. Holc, M. Kosec, Z. Trontelj, J. Pirnat, N. Dalal, V. Ramachandran, and J. Krzystek, J. Appl. Phys. **101**, 033901 (2007).
[11] W. Peng, N. Lemee, M. Karkut, B. Dkhil, V. Shvartsman, P. Borisov, W. Kleemann, J. Holc, M. Kosec, and R. Blinc, Appl. Phys. Lett. **94**, 012509 (2009).
[12] R. Martinez, R. Palai, H. Huhtinen, J. Liu, J. F. Scott, and R. S. Katiyar, Phys. Rev. B **82**, 134104 (2010).
[13] I. P. Raevski, M. S. Molokeev, S. V. Misyul, E. V. Eremin, A. V. Blazhevich, S. P. Kubrin, D. A. Sarychev, V. V. Titov, H. Chen, C.-C. Chou, S. I. Raevskaya, and M. A. Malitskaya, Ferroelectrics **475**, 52 (2015).
[14] T. Watanabe and K. Kohn, Phase Transitions **15**, 57 (1989).
[15] A. A. Gusev, S. I. Raevskaya, V. V. Titov, V. P. Isupov, E. G. Avvakumov, I. P. Raevski, H. Chen, C.-C. Chou, S. P. Kubrin, S. V. Titov, M. A. Malitskaya, D. A. Sarychev, V. V. Stashenko, and S. I. Shevtsova, Ferroelectrics **496**, 231 (2016).
[16] V. V. Laguta, V. A. Stephanovich, M. Savinov, M. Marysko, R. O. Kuzian, I. V. Kondakova, N. M. Olekhnovich, A. V. Pushkarev, Yu. V. Radyush, I. P. Raevski, S. I. Raevskaya, and S. A. Prosandeev, New J. Phys. **16**, 113041 (2014).
[17] B. Howes, M. Pelizzone, P. Fischer, C. Tabaresmunoz, J.-P. Rivera, and H. Schmid, Ferroelectrics **54**, 317 (1984).
[18] V. V. Laguta, A. N. Morozovska, E. A. Eliseev, I. P. Raevski, S. I. Raevskaya, E. I. Sitalo, S. A. Prosandeev, and L. Bellaiche, J. Mater. Sci. **51**, 5330 (2016).
[19] C. Tabares-Munoz, J.-P. Rivera, A. Bezinges, A. Monnier, and H. Schmid, Jpn. J. Appl. Phys. **24**, 1051 (1985).
[20] V. A. Murashov, D. N. Rakov, N. A. Ekonomov, A. K. Zvezdin, and I. S. Dubenko, Sov. Phys. Solid State **32**, 1255 (1990).
[21] D. Lebeugle, D. Colson, A. Forget, M. Viret, A. M. Bataille, and A. Gukasov, Phys. Rev. Lett. **100**, 227602 (2008).
[22] D. Rahmedov, S. Prosandeev, J. Iniguez, and L. Bellaiche, Phys. Rev. B **88**, 224405 (2013).
[23] E. A. Dul'kin, I. P. Raevskii, and S. M. Emel'yanov, Phys. Solid State **39**, 316 (1997).

[24] I. P. Raevskii, S. T. Kirillov, M. A. Malitskaya, V. P. Filippenko, S. M. Zaitsev, and L. G. Kolomin, Inorg. Mater. **24**, 217 (1988).
[25] M. M. Kumar, A. Srinivas, S. V. Surynarayana, G. S. Kumar, and T. Bhimasankaram, Bull. Mater. Sci. **21**, 251 (1998).
[26] S. L. Hou and N. Bloembergen, Phys. Rev. **138**, A1218 (1965).
[27] M. Fiebig, J. Phys. D: Appl. Phys. **38**, R123 (2005).
[28] T. Murao, Prog. Theor. Phys. **37**, 1038 (1967).
[29] I. P. Raevski, S. P. Kubrin, S. I. Raevskaya, V. V. Stashenko, D. A. Sarychev, M. A. Malitskaya, M. A. Seredkina, V. G. Smotrakov, I. N. Zakharchenko, and V. V. Eremkin, Ferroelectrics **373**, 121 (2008).
[30] R. O. Kuzian, I. V. Kondakova, A. M. Daré, and V. V. Laguta, Phys. Rev. B **89**, 024402 (2014).
[31] N. A. Pertsev, A. G. Zembilgotov, and A. K. Tagantsev, Phys. Rev. Lett. **80**, 1988 (1998).
[32] B. K. Ponomarev, E. Stiep, H. Wiegelmann, A. G. M. Jansen, W. Wyder, and B. S. Red'kin, Phys. Solid State **42**, 734 (2000).
[33] A. I. Kharkovskiy, Yu. V. Shaldin, and V. I. Nizhankovskii, J. Appl. Phys. **119**, 014101 (2016).
[34] J.-P. Rivera and H. Schmid, J. Appl. Phys. **70**, 6410 (1991).
[35] A. K. Zvezdin, G. P. Vorob'ev, A. M. Kadomsteva, Yu. F. Popov, D. V. Belov, and A. P. Pyatakov, J. Exp. Theor. Phys. **109**, 221 (2009).
[36] S. A. Ivanov, R. Tellgren, H. Rundlof, N. W. Thomas, and S. Ananta, J. Phys.: Condens. Matter **12**, 2393 (2000).
[37] S. A. Prosandeev, I. P. Raevski, S. I. Raevskaya, and H. Chen, Phys. Rev. B **92**, 220419(R) (2015).